Molecular-dynamics simulation of the smectic-A^* twist grain-boundary phase

Michael P. Allen and Mark A. Warren
H. H. Wills Physics Laboratory, University of Bristol, Royal Fort, Tyndall Avenue, Bristol, BS8 1TL, United Kingdom

Mark R. Wilson
Department of Chemistry, University of Durham, South Road, Durham, DH1 3LE, United Kingdom
(Received 6 August 1997)

In this paper we present the results of extensive molecular-dynamics simulations of a model of liquid crystals, in which a twist is imposed on the direction of preferred orientation. On quenching the system from a twisted nematic phase to a state point within the smectic-*A* phase, we observe a structure which corresponds closely to that of the smectic-A^* twist grain-boundary phase. We investigate this structure by means of director and structure factor profiles, and also develop a technique for automatically locating screw dislocations. Applying this technique to the configurations from our simulations, we obtain a defect distribution which is in qualitative agreement with theoretical predictions. [S1063-651X(98)02505-7]

PACS number(s): 61.30.Cz, 61.30.Jf, 61.20.Ja, 83.20.Jp

I. INTRODUCTION

In 1989, Renn and Lubensky (RL) predicted the occurrence of a novel liquid crystalline phase in systems of chiral mesogens, the twist grain-boundary (TGB) phase [1]. This discovery, together with the first experimental observation of the phase which was made at around the same time [2], generated a great deal of interest. The RL theory was motivated by a close correspondence between the mathematical description of the normal-metal to superconductor transition and that of the nematic (N) to smectic-A (S_A) liquid crystal. Both transitions are described by a complex order parameter $\psi(\mathbf{r})$: in a superconductor this is the complex amplitude of Cooper pairs, and in a smectic liquid crystal it represents the periodic modulation of the nematogen density, corresponding to the layers. In the latter case, the deviation of the local single-particle density from its average value is

$$\rho(\mathbf{r}) - \langle \rho \rangle = \psi(\mathbf{r}) + \psi^*(\mathbf{r}),$$

i.e., it is real, but characterized by an amplitude and a phase. Phenomenological mean field theories of a superconductor in zero magnetic field, and the $N \rightarrow S_A$ transition for uniaxial molecules, are based on a free energy functional $\mathcal{F}[\psi(\mathbf{r})]$ of the order parameter. Imposing the relevant symmetry on this functional (gauge invariance in the case of superconductivity, rotational invariance in liquid crystals) leads to identical mathematical forms for $\mathcal{F}[\psi(\mathbf{r})]$, so there is complete correspondence between the theories. RL extended the superconducting analogy to include the effects of molecular chirality. In doing so, they discovered the S_A^* TGB phase. This is the liquid crystalline analog of the Abrikosov flux lattice occurring in weakly correlated (type II) superconductors. The phase behavior (as a function of molecular chirality and temperature) depends on the penetration depth λ_2 and correlation length ξ, which are phenomenological constants in the RL theory. For a Ginzburg parameter $\kappa_G = \lambda_2/\xi > 1/\sqrt{2}$, the TGB phase intercedes between the chiral-nematic and smectic-*A* phases. The TGB phase, as illustrated in Fig. 1, consists of a set of domains along the twist axis. Within each domain there is smecticlike one-dimensional translational order, and the direction of preferred ordering, or director **n**, lies parallel to the layer normal **N**. At each domain boundary, however, both **n** and **N** undergo a discrete rotation through an angle $\Delta\theta$. This rotation is mediated by a set of equispaced, parallel screw dislocations with orientation between the layer normals on the two sides of the interface. These are topological defects in the ordering field ψ; on encircling one of the defects, one picks up a phase change of 2π in ψ, so that the arrangement of the smectic layers in the vicinity of each defect resembles a spiral. In the RL theory, the system is assumed infinite in the directions perpendicular to the twist, and the defects form a regular array of infinite lines a distance ℓ_d apart. The layer spacing remote from the defects is d_0. As the defect line is approached, the degree of translational ordering $|\psi|^2$ tends to zero over some radial distance $\approx \xi$. An idealized representation of the geometry of a single interface is shown in Fig. 2.

The first experimental evidence of the TGB phase [2] consisted of optical and x-ray studies of a series of chiral mesogens, which indicated the presence of both helical ori-

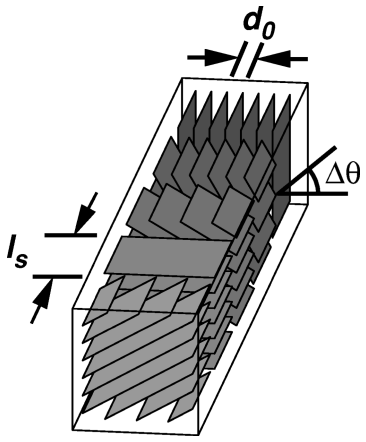

FIG. 1. Domain structure of the TGB phase, showing the grain boundary angle $\Delta\theta$, smectic domain width ℓ_s, and layer spacing d_0.

 © 1998 The American Physical Society

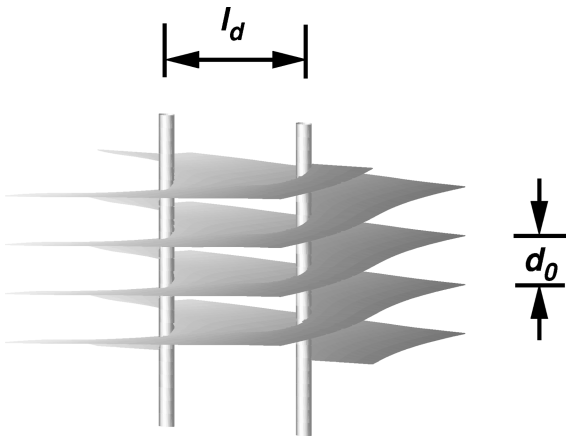

FIG. 2. Idealized structure of an interface between two domains in the TGB phase, showing the separation ℓ_d between screw dislocation defects.

entational order and smectic order. Subsequent experiments [3–5] probed the temperature dependence of the chiral pitch, and measured the static structure factor, hence providing an estimate of the smectic layer spacing, a lower bound on the range of translational correlations within smectic domains, and the width of domain boundaries. Finally, electron micrographs of freeze fracture specimens [6] provided estimates of the grain boundary angle $\Delta\theta$ and the defect spacing ℓ_d.

The possibility of twist grain boundaries in *achiral* liquid crystals was first suggested by Patel [7] in relation to experiments on a liquid crystal in a twist cell, i.e., in a sample bounded by plates favoring molecular alignment along the x direction on the top surface and along y on the bottom surface. The twist in the director field about the z axis induced by the director pinning can be detected as a nonzero transmitted intensity when the cell is placed between crossed polarizers. Patel found that the twist persists below the normal $N \rightarrow S_A$ transition temperature T_{NA}, while at the same time the presence of focal conic textures suggested smecticlike ordering. Strain-induced TGB structures have also been observed in suspensions of the bacteriophage fd [8]. The length of fd particles, about 8800 Å, is sufficient to allow direct observation of the block domains via differential interference contrast microscopy.

Several approaches to modeling of the TGB system might be considered. One of these would be to attempt an exact numerical solution of the mean field theory, i.e., minimization of the RL free energy functional $\mathcal{F}[\psi]$. Even in mean field theory, the detailed phase behavior (i.e., the dependence of the parameters ℓ_d, ℓ_s, and $\Delta\theta$ in Figs. 1 and 2 on temperature and molecular chirality) can be calculated only approximately by analytical methods [1]. In principle, lattice simulations could be used to determine the mean field phase diagram exactly, although this would be computationally expensive.

Our approach is somewhat different. Instead of using a coarse-grained model, we carry out molecular dynamics (MD) on a system of particles which incorporates the essential features of chirality and anisotropic interactions. We restrict our attention to a small number of state points, and look for evidence of TGB formation. Molecular dynamics is preferred to Monte Carlo simulation, partly because it allows access to dynamical properties (although here we concentrate mainly on analyzing static structure), and partly because of the comparative ease and efficiency with which MD can be parallelized. The majority of our simulations were carried out on the Edinburgh T3D parallel supercomputer, using the domain decomposition MD program GBMEGA [9]. The molecular model employed is the well-known Gay-Berne potential [10]. Chirality is imposed as in a twist cell, by the use of specially modified periodic boundary conditions. Large system sizes are employed to allow the use of a realistic degree of twist, and reduce the effects of the boundary conditions in the directions perpendicular to the twist axis. The translational and orientational ordering we observe in our system correspond qualitatively with the RL picture, and so we believe that this work represents the first computer simulation of the twist grain boundary phase. A particularly interesting aspect of the TGB structure is the topology of the smectic layers at the interface between regions of different smectic orientations. In the RL theory, each interface contains a regular array of twist defects. We have developed a technique for searching through molecular configurations for this kind of defect, and have found several convincing examples in configurations at the lowest two temperatures we studied. We have attempted to characterize the ordering in the neighborhood of these defects.

The organization of this paper is as follows. In Sec. II, we give details of the model and simulation techniques used. The TGB phase is distinguished by the behavior of the molecular orientation and smectic layer normal as a function of distance along the twist direction. In Sec. III, we define the profiles of nematic order parameter and structure function which we use to characterize this behavior, and present these results for each of the state points studied. This is followed in Sec. IV by a discussion of diffusion profiles, which we measure primarily to check that no parts of the system have solidified. In Sec. V, we describe our simulated annealing technique for finding defects in molecular configurations, and apply this to investigating the structure of the domain boundaries. We conclude in Sec. VI with a summary of our results, some comparisons with experiment, and possible directions for future work.

II. SIMULATION METHOD

A. Definition of model

A fully atomistic simulation of a system of chiral mesogenic molecules is clearly out of the question, certainly for the system size needed in order to study the TGB phase. The use of a soft potential is preferred over reference hard-particle systems such as spherocylinders, since parallelization of hard-particle MD is difficult. We choose the well-known Gay-Berne (GB) model [10]. In this model, molecules are represented by single sites, each with an orientation vector $\mathbf{e}_i$ and position vector $\mathbf{r}_i$, $i=1,\ldots,N$, which interact via an anisotropic pair potential,

$$v^{\mathrm{GB}}(\mathbf{e}_i,\mathbf{e}_j,\mathbf{r}_{ij}) = 4\varepsilon(\mathbf{e}_i,\mathbf{e}_j,\hat{\mathbf{r}}_{ij})\{\varrho^{-12}-\varrho^{-6}\},$$

$$\varrho = \frac{r_{ij}-\sigma(\mathbf{e}_i,\mathbf{e}_j,\hat{\mathbf{r}}_{ij})+\sigma_0}{\sigma_0}.$$

The diameter function σ depends on the relative orientations of the molecules and the unit vector $\hat{\mathbf{r}}_{ij}=\mathbf{r}_{ij}/r_{ij}$:

$$\sigma(\mathbf{e}_i,\mathbf{e}_j,\hat{\mathbf{r}}_{ij})=\sigma_0\left\{1-\frac{\chi}{2}\left[\frac{(\mathbf{e}_i\cdot\hat{\mathbf{r}}_{ij}+\mathbf{e}_j\cdot\hat{\mathbf{r}}_{ij})^2}{1+\chi\mathbf{e}_i\cdot\mathbf{e}_j}+\frac{(\mathbf{e}_i\cdot\hat{\mathbf{r}}_{ij}-\mathbf{e}_j\cdot\hat{\mathbf{r}}_{ij})^2}{1-\chi\mathbf{e}_i\cdot\mathbf{e}_j}\right]\right\}^{-1/2},$$

with shape anisotropy parameter $\chi=(\kappa^2-1)/(\kappa^2+1)$; $\kappa=\sigma_{ee}/\sigma_{ss}$. Here, $\sigma_{ss}=\sigma_0$ is the side-by-side diameter, and σ_{ee} the end-to-end diameter. The well-depth function ε also depends on the relative orientations of the two molecules, and takes the form

$$\varepsilon(\mathbf{e}_i,\mathbf{e}_j,\hat{\mathbf{r}}_{ij})=\varepsilon_0[\varepsilon'(\mathbf{e}_i,\mathbf{e}_j,\hat{\mathbf{r}}_{ij})]^{\mu}\times[\varepsilon''(\mathbf{e}_i,\mathbf{e}_j)]^{\nu},$$

$$\varepsilon'(\mathbf{e}_i,\mathbf{e}_j,\hat{\mathbf{r}}_{ij})=1-\frac{\chi'}{2}\left[\frac{(\mathbf{e}_i\cdot\hat{\mathbf{r}}_{ij}+\mathbf{e}_j\cdot\hat{\mathbf{r}}_{ij})^2}{1+\chi'\mathbf{e}_i\cdot\mathbf{e}_j}+\frac{(\mathbf{e}_i\cdot\hat{\mathbf{r}}_{ij}-\mathbf{e}_j\cdot\hat{\mathbf{r}}_{ij})^2}{1-\chi'\mathbf{e}_i\cdot\mathbf{e}_j}\right],$$

$$\varepsilon''(\mathbf{e}_i,\mathbf{e}_j)=[1-\chi^2(\mathbf{e}_i\cdot\mathbf{e}_j)^2]^{-1/2},$$

with well-depth anisotropy parameters $\chi'=(\kappa'^{1/\mu}-1)/(\kappa'^{1/\mu}+1)$; $\kappa'=\varepsilon_{ss}/\varepsilon_{ee}$. The two quantities ε_{ss} and ε_{ee} are, respectively, the side-by-side and end-to-end well depths. Throughout this paper we use σ_0 and ε_0 to define reduced units of length and energy, i.e., effectively we set $\sigma_0=1$ and $\varepsilon_0=1$. The corresponding unit of temperature is ε_0/k_B, where k_B is Boltzmann's constant. In the same way, we set the molecular mass $m=1$ and the combination $\sqrt{m\sigma_0^2/\varepsilon_0}$ defines a reduced unit of time.

It is usual to apply a spherical cutoff r_{cut}, and so in practice one uses the cut and shifted Gay-Berne potential

$$v(\mathbf{e}_i,\mathbf{e}_j,\mathbf{r}_{ij})=\begin{cases}v^{GB}(\mathbf{e}_i,\mathbf{e}_j,\mathbf{r}_{ij})-v^{GB}(\mathbf{e}_i,\mathbf{e}_j,r_{cut}\hat{\mathbf{r}}_{ij}), & r_{ij}\leqslant r_{cut}\\ 0, & r_{ij}>r_{cut}.\end{cases}$$

The phase diagrams of several variants of this model have been extensively studied [11–13]. The version we use here is $\kappa=4.4$, $\kappa'=20$, $\mu=1$, and $\nu=1$, with a spherical cutoff at $r_{cut}=5.5\sigma_0$. This particular parametrization is somewhat peculiar in that the well depth at the equilibrium separation in the side-by-side arrangement is less than for the end-to-end and side-to-end configurations. We choose it since previous studies [14] showed that there is a large region in the phase diagram where the smectic-*A* phase is stable. At the chosen reduced density of $\rho\sigma_0^3=0.16$, the phase transitions occur at the following reduced temperatures $T^*=k_BT/\varepsilon$:

$$\text{Isotropic} \xrightarrow{T^*=1.6} \text{Nematic} \xrightarrow{T^*=1.1} \text{Smectic} \xrightarrow{T^*=0.6} \text{Solid}.$$

The Gay-Berne potential itself is achiral and, on its own, will not lead to any chiral phases. In principle, molecular chirality could be introduced explicitly, by adding a chiral term to the site-site potential, or by rigidly joining Gay-Berne units to form chiral ''molecules.'' The problem with this approach is that in any computer simulation of a phase with long range chiral ordering (such as the twisted nematic or TGB phases which interest us), the periodic boundary conditions restrict the chiral pitch λ to a discrete set of values (fractions of the box length). These values will not, in general, match the equilibrium value of the pitch for a given molecular structure at the chosen state point, in the thermodynamic limit. Moreover, states of very different pitch are separated by a large free energy barrier, so that transitions between them will be rare events. One way in which these problems might be overcome would be to allow the dimensions of the simulation box to change continuously, for instance by using Nosé-Hoover volume dynamics or by incorporating constant pressure Monte Carlo moves [15]. In practice, we rejected these methods, since long equilibration times would still be required, and a continually changing box shape would make it harder to define and average the spatial profiles we need to characterize the ordering in the twisted system. Instead, we use the twist-cell geometry with an achiral molecular model: we prepare a uniformly twisted configuration with a chiral pitch consistent with the periodic boundary conditions. Although an untwisted state of lower energy exists (with the director pointing along the original twist axis), the chiral axis and pitch can usually be maintained indefinitely, since escape of the director field toward uniform alignment involves crossing a free energy barrier of states with large splay or bend energy. As we shall see, this stability holds for the variant of the Gay-Berne potential we use here.

We make use of *twisted periodic boundary conditions* (TPBC's): each periodic image of the cuboidal simulation cell along the z axis is rotated through $\pi/2$ with respect to the last [16]. This rotation is incorporated into the calculation of the forces between pairs of particles in different periodic images, and also when replacing particles which have left the basic cell in the $\pm z$ directions. In the latter case, the vectors describing the particle velocity and angular velocity are rotated, as well as the position and orientation.

B. System size, state points, and run details

An important determinant of the physical realism of our model is the ratio of the pitch to the smectic layer spacing, λ/d_0. This quantity varies widely among different experimental systems. In studies of the fd virus [8], $\lambda/d_0\approx 10$, but these are flexible, highly elongated particles with a length-to-diameter ratio $L/D\approx 130$. In the original experiments on mesogenic molecules [2], typically $\lambda/d_0\approx 100$. Our particle model has length-to-width ratio ≈ 4.4, much closer to the molecular value than to one appropriate for fd, and the smectic layer spacing is of order $d_0\approx 4\sigma_0$. We use a cuboidal box with sides L_x, L_y, and L_z; the TPBC's require equal transverse box lengths $L_x=L_y\equiv L_\perp$. We set $L_z\approx 80\sigma_0$, so that the pitch is $\lambda=320\sigma_0$, i.e., $\lambda/d_0\approx 80$, in reasonable correspondence with the molecular experiments. The principal effect of finite $L_\perp$ is to restrict the number and orientation of accessible smectic layers to a discrete set commensurate with the box. The transverse wave vectors $\mathbf{k}_\perp$ consistent with the periodic boundary conditions are

$$\mathbf{k}_\perp=\frac{2\pi}{L_\perp}(n_x\hat{\mathbf{x}}+n_y\hat{\mathbf{y}}), \tag{1}$$

where n_x and n_y are integers. In the RL theory, $L_\perp$ is assumed infinite, and the set of accessible wave vectors is a continuum. This is also a good approximation for the experiments mentioned in Sec. I, in which the transverse sample

dimensions are large. It is important to make $L_\perp$ reasonably large in the simulations, since we shall be examining the structure factor as a function of z for evidence of TGB formation, and want to be sure that any separation we see into smectic domains with distinct orientations is a real effect and not simply an artifact of the boundary conditions. In fact, we performed two independent sets of simulations, one with $L_\perp = L_z/2 \approx 40\sigma_0$, and the other doubled in the x and y directions, i.e., with $L_\perp = L_z \approx 80\sigma_0$. The corresponding system sizes are $N = 21\,000$ and $N = 84\,000$. We studied two temperatures above T_{NA} for the untwisted system, and three below it.

The starting configurations for the runs were prepared in the following manner. $N = 5250$ particles were placed on the sites of a simple cubic lattice at a low density ($\rho\sigma_0^3 = 0.02$) in a box with relative dimensions 1:1:4, their orientations lying in the xy plane and uniformly twisting along the z axis. The particles were each given random initial displacements of 0.1 lattice spacing, and a rotation about a random direction through an angle up to 0.3 rad. The system was gradually compressed to the required density, $\rho\sigma_0^3 = 0.16$. This was done using an MD run, with isotropic rescaling of coordinates at regular intervals. A constant kinetic temperature $T^* = 1.4$ was maintained through scaling of angular and translational velocities at each time step. In reduced units, the time step was $\Delta t = 0.0025$. Throughout this procedure, the twisted orientational ordering was maintained using an extra field

$$v_{\text{align}} = v_0 \sum_{i=1}^{N} \{\tfrac{3}{2}[\mathbf{e}_i \cdot \mathbf{n}(z_i)]^2 - \tfrac{1}{2}\},$$

with

$$\mathbf{n}(z) = \cos\left(\frac{\pi z}{2L_z}\right)\hat{\mathbf{x}} + \sin\left(\frac{\pi z}{2L_z}\right)\hat{\mathbf{y}}.$$

As the density increased, the magnitude of the field was progressively reduced so as to maintain the overall nematic order parameter (defined in Sec. III) within 10% of the known value for the untwisted system at this state point. The system was equilibrated for a further 50 000 steps with no external field, to check for any instability toward an untwisted state. $2\times2\times1$ periodic images were combined to produce a 21 000-particle configuration with box sides in the ratio 1:1:2, which was used as the starting point for further runs. The final configuration from the $T^* = 1.4$ simulations was doubled up again in the xy directions to produce the cubic starting configuration for the 84 000-particle runs.

A summary of the run parameters and lengths of these runs is shown in Table I. In the set of runs with $N = 21\,000$, the simulations at $T^* = 0.8$ and 0.9 were both started from the final configuration at $T^* = 1.0$. With this exception, all the runs were contiguous in order of decreasing temperature. During each run, the temperature was maintained constant by periodically rescaling translational and angular velocities. We monitored the evolution of the orientational and structure profiles, to be defined in Sec. III, and allowed the profiles to relax to a state from which there did not seem to be any further qualitative change. This does not necessarily imply that an equilibrium state has been reached: as we shall see, the time scale for the motion of boundaries between differently ordered regions is very long. Ideally, to check equilibration one would carry out several independent quenches from the twisted nematic phase, but this is very expensive. A measure of confidence in the validity of our results can be obtained by comparing the independent simulations of the two different sized systems. We return to this in Sec. VI.

TABLE I. Simulation details.

N	21 000	84 000
$L_\perp$	40.34	80.67
$L_\parallel$	80.67	80.67
T^*	Run length/1000 steps	
1.4	40	50
1.2	—	40
1.0	120	60
0.9	230	65
0.8	100	—

III. ORIENTATIONAL AND TRANSLATIONAL ORDER

A. Definitions

We now define the functions we use to characterize the variation of the orientational and translational ordering along the twist direction, z. We assume that any domain boundaries that form are oriented perpendicular to z, in accordance with theory and experiment; our results will show that this is indeed the case.

To characterize the orientational order, we use profiles of the second-rank order tensor. These are calculated in the usual way, as averages over the particles lying within each profile bin of specified width δz around z_{bin}:

$$Q_{\alpha\beta}(z_{\text{bin}}) = \frac{1}{N_{\text{bin}}} \sum_i \left\{\frac{3}{2} e_{i\alpha} e_{i\beta} - \frac{1}{2}\delta_{\alpha\beta}\right\} \Delta(z_i - z_{\text{bin}}),$$

$$\alpha, \beta = x, y, z,$$

$$\Delta(z_i - z_{\text{bin}}) = \begin{cases} 1 & \text{when } |z_i - z_{\text{bin}}| \leqslant \delta z/2 \\ 0 & \text{otherwise,} \end{cases}$$

and $N_{\text{bin}} = \Sigma_i \Delta(z_i - z_{\text{bin}})$ is the number of molecules falling within this range. We choose values of z_{bin} at intervals δz. We then diagonalize $Q_{\alpha\beta}(z_{\text{bin}})$ to obtain the nematic order parameter $P_2(z_{\text{bin}})$ (the highest eigenvalue) and the director $\mathbf{n}(z_{\text{bin}})$ (the corresponding eigenvector) as functions of z_{bin}. Generally, $\mathbf{n}$ is close to the xy plane. The orientation within this plane is defined by

$$\theta_{\mathbf{n}}(z_{\text{bin}}) = \tan^{-1}\left(\frac{n_y(z_{\text{bin}})}{n_x(z_{\text{bin}})}\right).$$

The overall order parameter for the system is obtained by averaging $P_2(z_{\text{bin}})$ over all $n_{\text{bins}} = L_z/\delta z$ bins:

$$\overline{P_2} = \frac{1}{n_{\text{bins}}} \sum_{\text{bin}=1}^{n_{\text{bins}}} P_2(z_{\text{bin}}).$$

The definition of profiles for characterizing translational ordering is slightly more subtle. In an untwisted smectic, the appropriate quantity to measure would be the structure factor,

$$S(\mathbf{k}) = \langle |\rho(\mathbf{k})|^2 \rangle, \tag{2}$$

$$\rho(\mathbf{k}) = \frac{1}{\sqrt{N}} \sum_{i=1}^{N} \exp(i\mathbf{k}\cdot\mathbf{r}_i).$$

In a well-ordered smectic phase, this function has a large peak at the wave vector $\mathbf{k}=(2\pi/d_0)\mathbf{N}$, where $\mathbf{N}$ is the unit layer normal, and d_0 is the smectic layer spacing. We are interested in how $\mathbf{N}$, d_0, and the height of the peak vary along the twist direction. In the TGB phase, we expect $\mathbf{N}$ in each domain to be colinear with the director, and so we confine our attention to transverse wave vectors $\mathbf{k}_\perp$, for which $k_z=0$. We calculate the structure factor within profile bins

$$S(\mathbf{k}_\perp ; z_{\rm bin}) = \langle |\rho(\mathbf{k}_\perp ; z_{\rm bin})|^2 \rangle,$$

$$\rho(\mathbf{k}_\perp ; z_{\rm bin}) = \frac{1}{\sqrt{N_{\rm bin}}} \sum_i \exp(i\mathbf{k}_\perp \cdot \mathbf{r}_i) \Delta(z_i - z_{\rm bin}),$$

defined as before for a grid of transverse wave vectors compatible with the periodic boundary conditions, given by Eq. (1), up to maximum values $k_x, k_y \approx 2\pi/\sigma_0$. Within well-ordered domains, the first-order peaks in $S(\mathbf{k}_\perp ; z_{\rm bin})$ lie on a ring of radius $k_0 = 2\pi/d_0$, and we are interested mainly in their angular position. In order to represent this dependence, we map our data from the (k_x, k_y) plane to polar coordinates (k, θ), and integrate over a k shell about k_0, to obtain a layer orientation profile $S(\theta; z_{\rm bin})$. The average of $S(\mathbf{k}_\perp ; z_{\rm bin})$ over profile bins,

$$\overline{S}(\mathbf{k}_\perp) = \frac{1}{n_{\rm bins}} \sum_{\rm bin=1}^{n_{\rm bins}} S(\mathbf{k}_\perp ; z_{\rm bin}),$$

is also informative. This is *not* the same as the structure factor for the whole system [Eq. (2)], but gives qualitatively similar information on the prevalence of fluctuations toward smectic ordering at different wave vectors.

We use 40 bins for all our profiles, so that each bin is approximately $2\sigma_0$ in width and contains on average around 500 particles for the $N=21\,000$ system, and 2000 for the $N=84\,000$ system. To improve statistics, we averaged the profiles over several successive configurations. In the discussion of the results, we drop the suffix ''bin'' from the z coordinate $z_{\rm bin}$.

B. Results

$T^*=1.4$ is well above T_{NA} for the untwisted system, and so we expect to observe twisted nematic order, but no long-range smecticlike order. The absence of well-ordered smectic regions is revealed in the bin-averaged structure factor shown in Fig. 3(a). At this statepoint, the function is radially symmetric, with a broad, low peak at around $k\sigma_0 = 1.7$; we find that the radial dependence for the two system sizes is the same. Profiles of the director orientation $\theta_{\mathbf{n}}(z)$ [Fig. 4(a)] show that $\mathbf{n}(z)$ rotates uniformly from one end of the simulation box to the other. The degree of nematic ordering is quite low: $\overline{P_2} \approx 0.40$. There is no sign of any escape of the director toward a uniformly aligned state $\mathbf{n}=\hat{\mathbf{z}}$; on average, the absolute angle that $\mathbf{n}(z)$ makes with the xy plane is $\approx 9°$ or less throughout the runs for both system sizes.

On cooling to $T^*=1.2$ the qualitative behavior of the director profile remains unaltered, although now the nematic order parameter has increased to $\overline{P_2}=0.59$. The profile-averaged structure factor $\overline{S}(\mathbf{k}_\perp)$ (not shown) retains its axial symmetry, but the peak is markedly narrower and higher than at $T^*=1.4$. We also observe a slight shift of the peak toward lower k. While the bin-averaged structure factor is independent of θ, at a given z the fluctuations toward translational ordering are predominantly along the local director. This correlation between local translational and orientational ordering can be seen in Fig. 5(a), in which the shading shows the orientational dependence of the structure profile $S(\theta; z)$, and the dotted line is the transverse director profile $\theta_{\mathbf{n}}(z)$.

At $T^*=1.0$, which lies just below T_{NA} for the untwisted system, there is a definite change in the structure. The profile-averaged structure factor [Fig. 3(b)], no longer has an axial symmetry. Instead, we see the emergence of sharp peaks at specific wave vectors, whose heights fluctuate slowly during the course of the run. This suggests that the system is attempting to form smectic domains. In the $N=21\,000$ system, we see some evidence of domain formation in the structure factor and director profiles [Fig. 4(b)]. The angular variation of $\mathbf{n}$ and $\mathbf{N}$ with z is no longer uniform; however, there are no sharp domain interfaces. Examination of slices through the configurations shows that there are three fairly well-ordered smectic regions of distinct layer orientations, separated by boundary regions where the ordering is more nematiclike, which take up the twist. In each of these domains, the layer spacing $d_0 \approx 4.3\sigma_0$. In the $N=84\,000$ system, the height of the structure peaks grows more slowly, but after $\approx 40\,000$ steps the results resemble those of the smaller system [see Fig. 5(b)].

At $T^*=0.9$, the peaks in the bin-averaged structure factor which we observed at $T^*=1.0$ grow in height, as shown in Fig. 3(c). Much more interestingly, the director and structure profiles for the $N=21\,000$ runs [Fig. 4(c)], reveal very clear domain boundaries. For the particular configuration shown here, there are four domains, with boundaries at $z/\sigma_0 \approx 8$, 25, 33, and 60; at other parts of the run the smallest domain is not visible. The results from the independent quench from $T^*=1.0$ to 0.8 (not shown) are rather similar, except that the maximum values of $S(\mathbf{k}_\perp ; z)$ in the center of the domains are somewhat higher. The profiles for the $N=84\,000$ system [Fig. 5(c)], also show some nonuniformity in the director, although the boundaries are not so clearly delineated. These results are consistent with a TGB-like structure.

IV. DIFFUSION

Our principal motivation for studying single-particle dynamics is to verify that the ordered domains we observe are smecticlike, and not crystalline. The diffusion rate is a useful

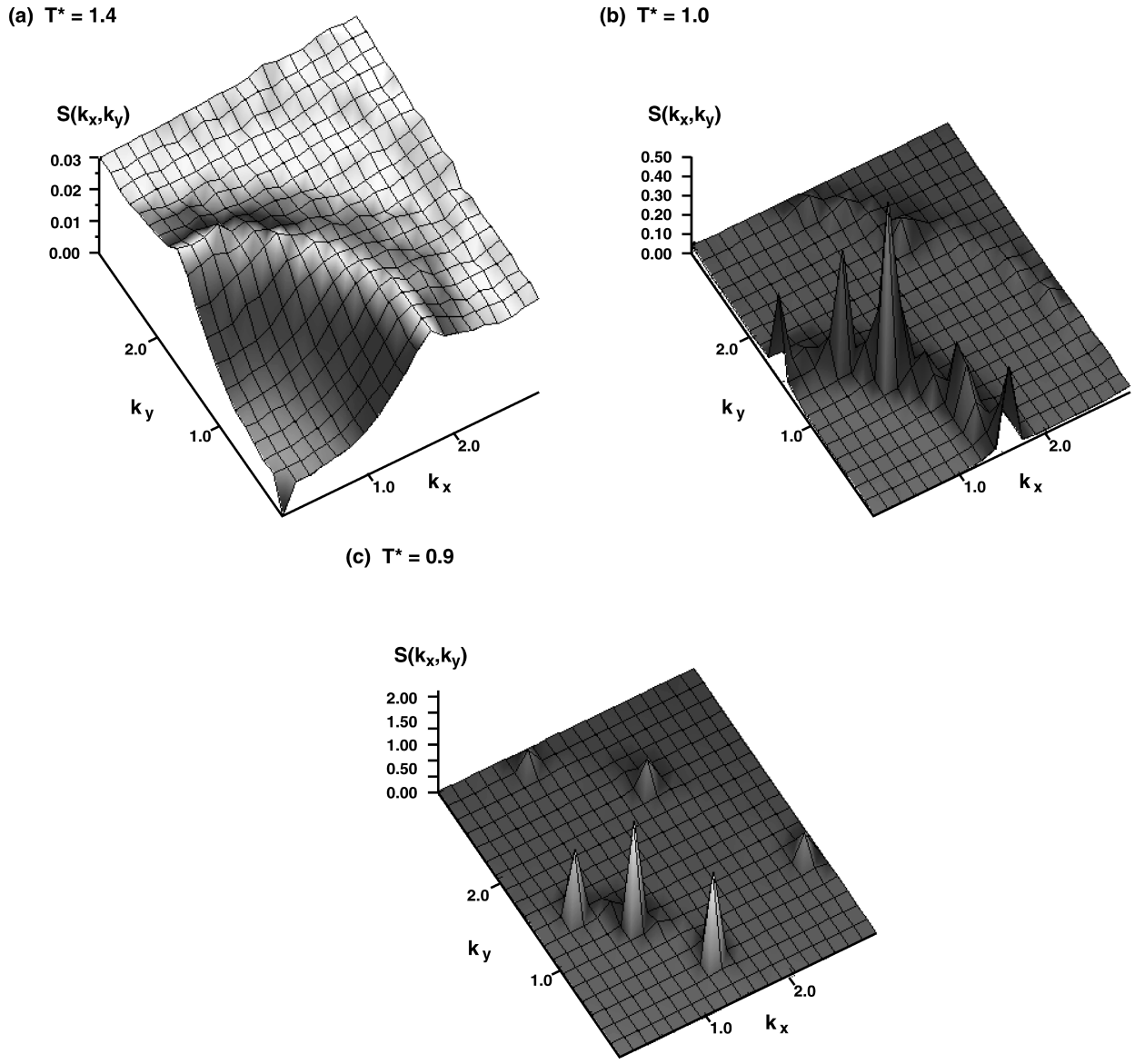

FIG. 3. The profile-averaged structure factor $\overline{S}(\mathbf{k}_\perp)$ for the $N=21\,000$ system. (a) $T^*=1.4$, (b) $T^*=1.0$, and (c) $T^*=0.9$. Here and henceforth we use dimensionless reduced units based on the Gay-Berne potential parameters σ_0 and ε_0, and the molecular mass m, as defined in the text.

indicator of whether or not the system has solidified. In a phase, for example smectic-*A* or nematic, with uniaxial symmetry about the director **n**, there are two coefficients $D_\perp$ and $D_\parallel$, which correspond to diffusion along and perpendicular to **n**. They can be defined through the Einstein relations describing the asymptotic behavior of the mean square displacement. The definition of diffusion coefficients in a twisted nematic or TGB phase is complicated by the inhomogeneity of the orientational order. In a system with spatially dependent director $\mathbf{n}(\mathbf{r})$, one can define, for each particle, the square displacements resolved along the local director evaluated at its initial position $\mathbf{r}(0)$,

$$r_\parallel^2(t)=\langle|(\mathbf{r}(t)-\mathbf{r}(0))\cdot\mathbf{n}(\mathbf{r}(0))|^2\rangle,$$

and similarly $r_\perp^2(t)=r^2(t)-r_\parallel^2(t)$ for motion perpendicular to the director. In principle, if $\mathbf{n}(\mathbf{r})$ varies sufficiently slowly in space and time, so that the linear diffusive regime is reached before the particle strays into a region with a significantly different director, then values for $D_\perp$ and $D_\parallel$ can be calculated from these displacements. In order to demonstrate that the particles are diffusing, however, it is sufficient to calculate a profile of $\langle|\mathbf{r}(t)-\mathbf{r}(0)|^2\rangle$, i.e., the average *total* mean square displacement of particles which were in each of the 40 slabs at time $t=0$. The results for the $N=84\,000$ system at $T^*=0.9$ are shown in Fig. 6. The root mean square displacement over the entire run of 65 000 time steps ($t_{\max}=160$ in reduced units) is greater than $8\sigma_0$ in all of the profile bins, and the average over the bins is $8.8\sigma_0$. Since this is more than twice our estimated value of d_0, we conclude that, although the diffusion is quite slow, the system is certainly not a solid.

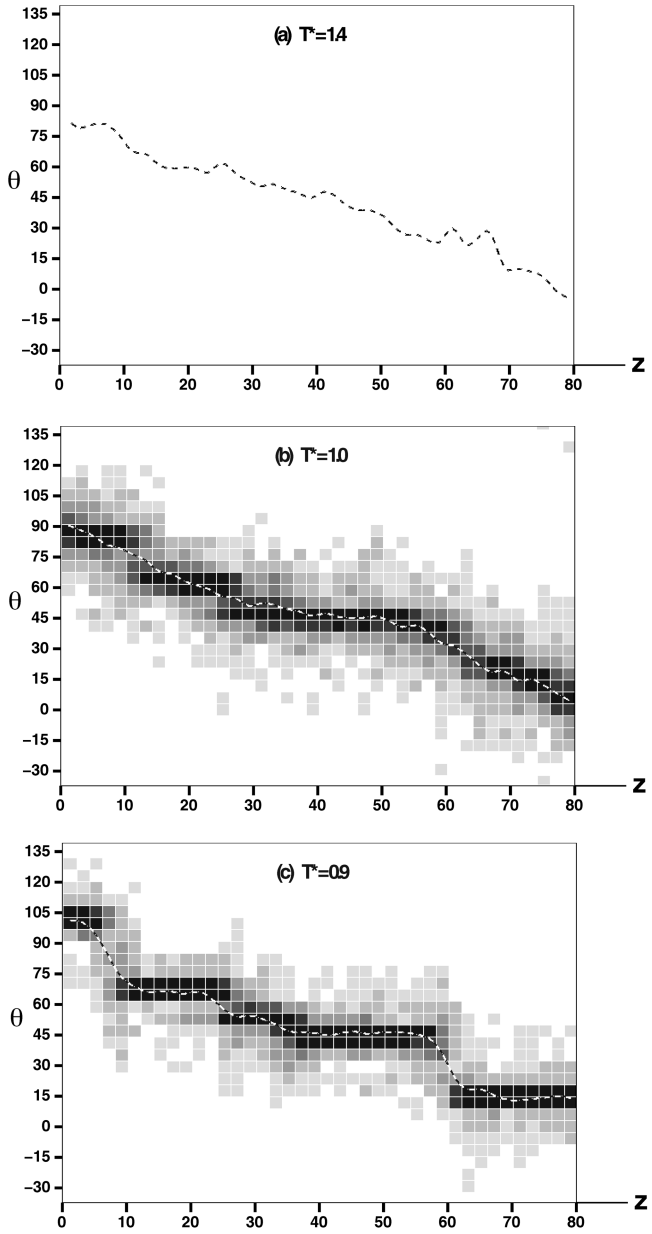

FIG. 4. Profiles showing the orientational dependence of the structure factor, $S(\theta;z)$ (darker shading indicates higher values, arbitrary units), and the director profile, $\theta_{\mathbf{n}}(z)$ (dotted line), for the simulations with $N=21\,000$. θ is measured in degrees, z in units of σ_0. In each case, the profiles are averaged over 1000 time steps, near the end of the run concerned. (a) $T^*=1.4$ (structure factor independent of θ and not shown). (b) $T^*=1.0$. (c) $T^*=0.9$.

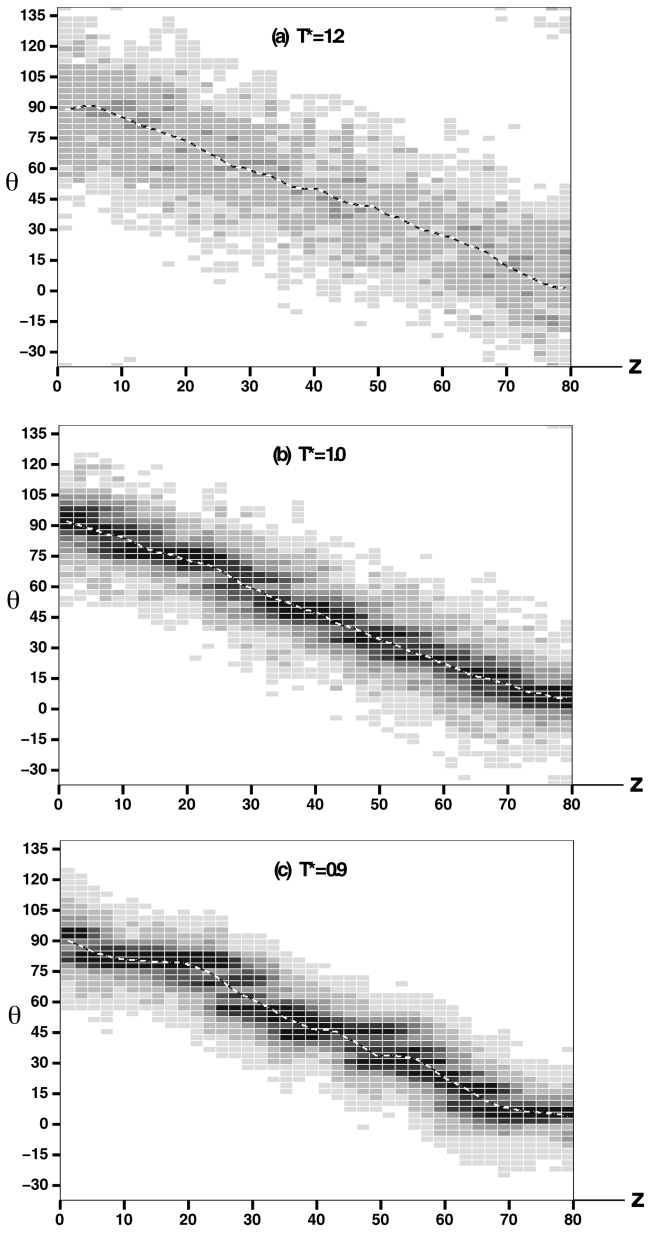

FIG. 5. Profiles showing the orientational dependence of the structure factor, $S(\theta;z)$ (darker shading indicates higher values, arbitrary units), and the director profile, $\theta_{\mathbf{n}}(z)$ (dotted line), for the simulations with $N=84\,000$. θ is measured in degrees, z in units of σ_0. In each case, the profiles are averaged over 1000 time steps, near the end of the run concerned. (a) $T^*=1.2$. (b) $T^*=1.0$. (c) $T^*=0.9$.

V. STRUCTURE OF INTERFACIAL REGIONS

Our orientational and structure profiles are consistent with the TGB structure, but they do not shed much light on the structure of the domain interfaces. Since these interfaces occupy only a small fraction of the sample volume, it is difficult to probe their structure in x-ray scattering experiments, and to date no direct experimental evidence for the presence of the twist defects predicted in the RL theory exists. Computer simulation allows us to investigate the domain boundaries much more closely. In this section we describe the techniques we use to search for defects, and compare the nature and distribution of defects seen in our simulations with the RL theory.

A. Configuration slices

Twist defects lying in the plane of the domain boundaries can be seen directly, by inspecting images of slices taken through the configurations, perpendicular to the twist axis. In Fig. 7, we show three successive slices, taken from the final configuration of the runs at $T^*=0.8$. Slices (a) and (c) both show more-or-less uninterrupted smectic ordering, in two

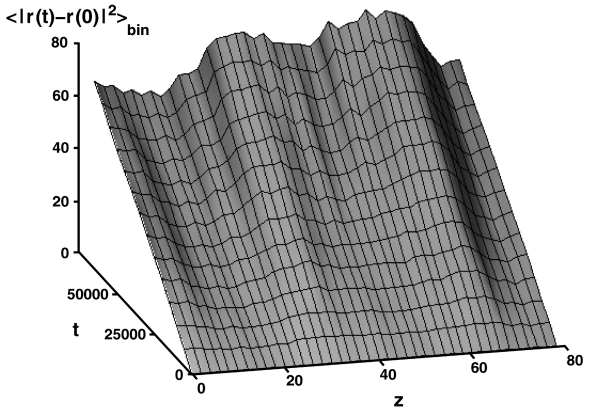

FIG. 6. Profiles of total mean squared displacement, at the temperature $T^*=0.9$, from the $N=84\,000$ run. Distances are in units of σ_0, and time t in time steps, $\Delta t=0.0025$.

different orientations, and a twist defect can be clearly seen running diagonally through the central slice (b). The orientations of the smectic layers above and below the layer are approximately 117° and 126°, so this defect creates a grain boundary with $\Delta\theta\approx 9°$.

Identifying defects in this way is tedious, and is particularly difficult if the defects do not lie in the plane of the slices. To overcome this problem, and allow a more systematic investigation of the defect distribution, we developed a method for searching for them automatically. Briefly, this works as follows: we define a *goal function* which gives a numerical measure of how well the ordering in the neighborhood of a given line segment conforms to the topology of twist defects shown in Fig. 2; then we seek to maximize this goal function over the space of possible segments.

B. Definition of goal function

In the RL theory, the defects are infinite straight lines in the xy plane, but we do not assume this. Rather, we represent them as chains of connected line segments Γ, unrestricted in orientation. The first step is to define a goal function for a single segment, $G(\Gamma)$. In cylindrical coordinates based on the line segment, (r,ϕ,ζ), with the ends of $G(\Gamma)$ at $\zeta=\pm\ell_\Gamma/2$, we define a particle number density which takes into account the twist, with specified wave number k, about the ζ axis:

$$\rho_d(\Gamma,k)=\int_{\mathcal{R}_\Gamma} d\mathbf{r}\ \rho(\mathbf{r})\ \exp[\mathrm{i}(k\zeta-\phi)], \tag{3}$$

where $\mathcal{R}_\Gamma$ is a cylindrical shell $r_{\min}<r<r_{\max}$, $|\zeta|<\pm\ell_\Gamma/2$. We then define $G(\Gamma)$ by taking the square modulus, normalizing by the number of particles within $\mathcal{R}_\Gamma$, and maximizing over k:

$$S_d(\Gamma,k)=\frac{|\rho_d(\Gamma,k)|^2}{\int_{\mathcal{R}_\Gamma} d\mathbf{r}\ \rho(\mathbf{r})},$$

$$G(\Gamma)=\max_k S_d(\Gamma,k).$$

By construction, $G(\Gamma)$ is greatest when Γ lies along a twist defect.

The density which appears in Eq. (3) is obtained by averaging over a number of successive configurations, to improve statistics. The rate of single-particle diffusion gives a conservative estimate of the length of time over which we can perform this averaging without smearing out the density modulation. In practice, the number of configurations is limited by the computational expense of calculating G, although this was reduced considerably by using a linked cell search to extract molecules lying within $\mathcal{R}_\Gamma$.

The arrangement of defects in the system is described as a set of chains of segments, or *conformation*, $\Omega\equiv\{\Gamma_i\}$. The major contribution, $\mathcal{G}'(\Omega)$, to the *global goal function* $\mathcal{G}(\Omega)$, is a sum of single-segment terms,

$$\mathcal{G}'(\Omega)=\sum_{i=1}^{n_{\mathrm{segs}}} G(\Gamma_i).$$

However, in order to obtain a well-defined optimization problem, several additional points must be considered. First, the evaluation of $G(\Gamma)$ is clearly meaningless if the segment is too short (comparable with the smectic layer spacing). We therefore impose a minimum length $\ell_{\min}$ on every segment. It is also convenient to impose a maximum $\ell_{\max}$, of the order of the periodic box dimensions. Next, we need to prevent the total length of the chains from growing without bound. While we do not know *a priori* the total length of defect, we estimate that it will be of the order $\pi L_\perp^2/2d_0$. This is the total length predicted on the basis of a regular network of twist defects producing a $\pi/2$ twist in the box. We therefore place an upper bound $L_{\max}\approx\pi L_\perp^2/2d_0$ on the total segment length. If the chains do not interact in any way, then several may choose to lie along the same defect. To inhibit this, we impose a limit on how close the line segments may approach each other. We imagine a hard spherocylinder $\mathcal{S}_\Gamma$ of radius $r_{\max}$ and length ℓ_Γ, coaxial with each Γ. Pairs of spherocylinders $(\mathcal{S}_{\Gamma_i},\mathcal{S}_{\Gamma_j})$ are permitted to overlap only if the corresponding (Γ_i,Γ_j) are neighboring segments on the same chain. Finally, we add a term $-\lambda n_{\mathrm{chains}}$ to the global goal function, favoring longer chains over a large number of isolated segments.

A precise definition of our problem is now possible: we must maximize

$$\mathcal{G}(\Omega)=\mathcal{G}'(\Omega)-\lambda n_{\mathrm{chains}}, \tag{4}$$

subject to the spherocylinder overlap constraint, along with the conditions

$$\ell_{\min}<\ell_{\Gamma_i}<\ell_{\max}\ \ \forall i \quad\text{and}\quad \sum_{i=1}^{n_{\mathrm{segs}}}\ell_{\Gamma_i}\leq L_{\max}. \tag{5}$$

C. Maximization of goal function

We use the *simulated annealing* method [17] to maximize $\mathcal{G}(\Omega)$ subject to the constraints, since Ω has both discrete and continuous degrees of freedom: the partitioning of segments among chains, and the positions of the nodes at which segments are connected. We choose a set of *annealing moves* $\mathcal{M}_1,\mathcal{M}_2,\ldots,\mathcal{M}_n$, each of which modifies the conforma-

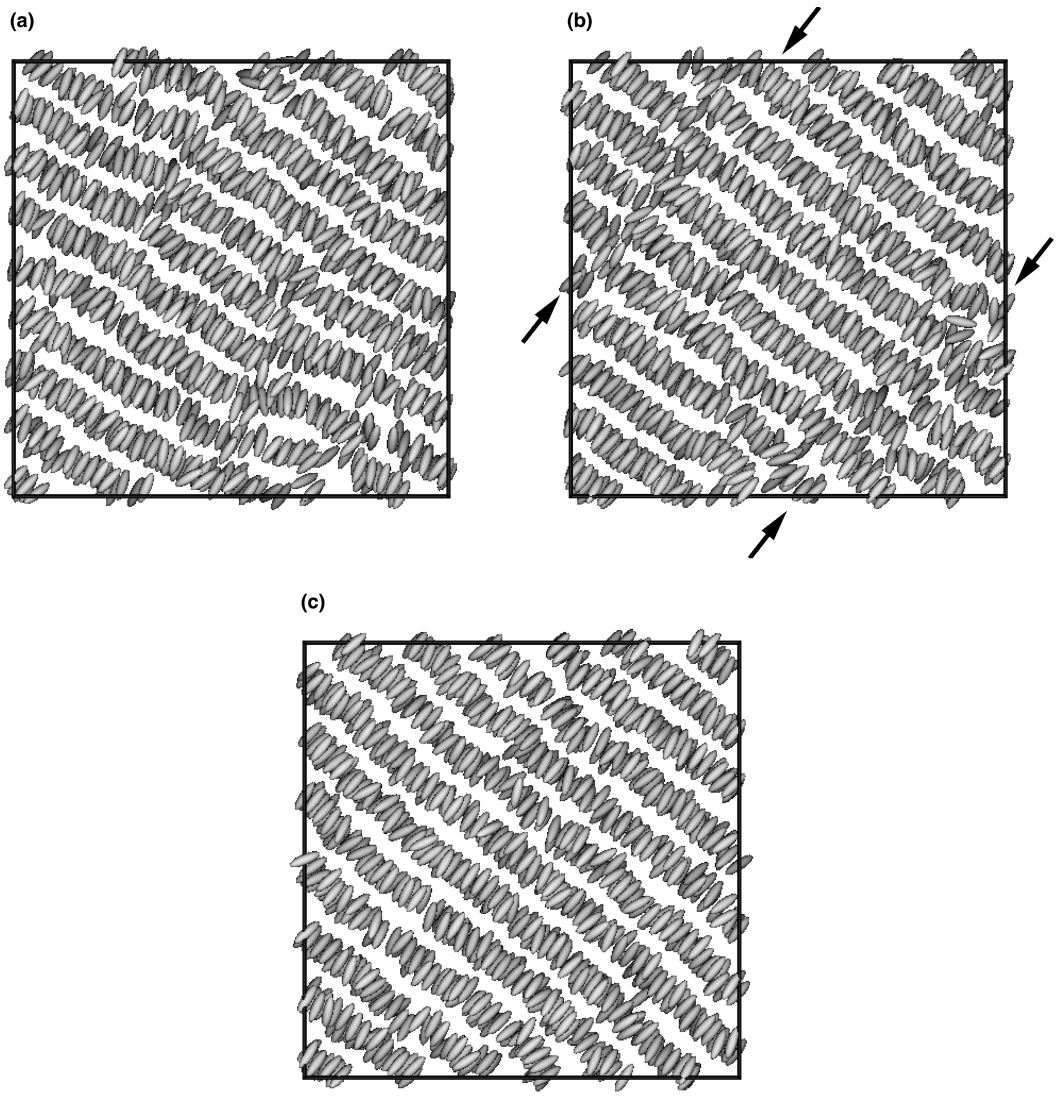

FIG. 7. Three successive slices of thickness $3.22\sigma_0$, perpendicular to the twist axis, from one of the configurations at the end of the run at $T^*=0.8$. The central slice contains a twist defect, running diagonally through the box, indicated by arrows. The molecules are reduced in size for clarity.

tion in some way. We begin with a random conformation Ω_0, and set the *annealing temperature* τ to some $\tau_0>0$. At each step s of the annealing process, we select one of the moves $\mathcal{M}_i$ at random, and apply it to the current conformation, generating a *trial* conformation $\Omega_{s+1}^{\text{trial}}=\mathcal{M}_i\Omega_s$. We then calculate the change in the goal function,

$$\Delta\mathcal{G}=\mathcal{G}(\Omega_{s+1}^{\text{trial}})-\mathcal{G}(\Omega_s).$$

If $\Delta\mathcal{G}>0$, then we accept the move, i.e., we set $\Omega_{s+1}=\Omega_{s+1}^{\text{trial}}$. If the trial conformation has a lower goal function, then we accept the move with a probability $\exp(\Delta\mathcal{G}/\tau)$; otherwise we retain the unmodified conformation $\Omega_{s+1}=\Omega_s$. Over the course of the run, the ''temperature'' τ is gradually reduced to zero, so that eventually only moves which increase the goal function are accepted. This procedure is guaranteed to find the global maximum provided that τ_0 is large enough, the moves are sufficiently general to allow exploration of the entire space of conformations consistent with the constraints, and τ is reduced sufficiently slowly.

The annealing moves we use, shown in Fig. 8, involve displacement of a node joining two segments, transferral of a segment from the end of one chain to another, and breaking a chain at a node. These three types were attempted with relative frequencies 10:1:1, respectively. The size of displacement moves was reduced adaptively as the temperature was lowered to maintain a constant acceptance rate of around 30%. We adopted a linear reduction of τ from τ_0 to zero for the annealing schedule. The other relevant parameters in the simulated annealing process were chosen somewhat empirically: their values are listed in Table II.

D. Results

The method outlined above successfully locates the defect which we found by eye, and many others. Moreover, independent annealing runs on a given density distribution starting from two different random conformations of unisegment chains give fairly repeatable results: the final conformations differ only in the positions of a few segments, and most of these clearly do not correspond to well-defined defects.

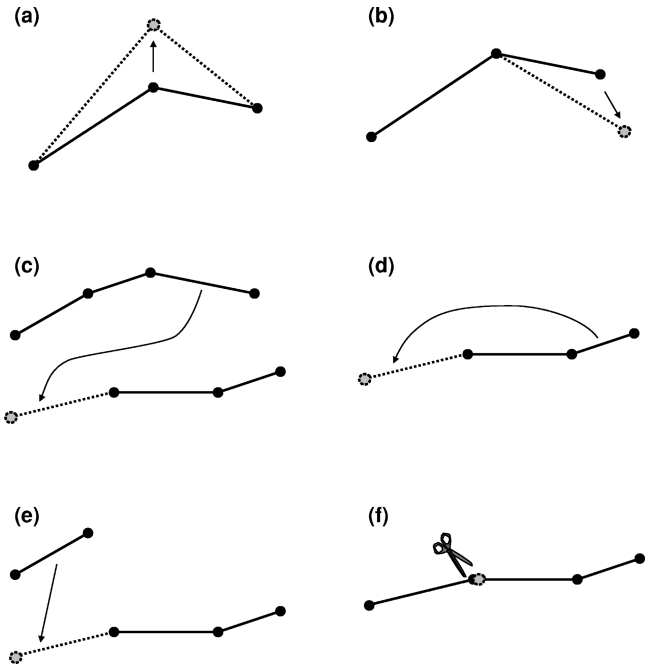

FIG. 8. Annealing moves for maximizing the goal function for detecting defects. *Displacement* of (a) an interior node, and (b) an end point. *Segment transfer* (c) from one chain to another, and (d) to the opposite end of the same chain. (e) *Destruction,* i.e., transfer from a one-segment chain. (f) *Disconnection:* a chain is broken at one of its interior nodes. None of the segment conformations are changed, but there is a decrease in the goal function since n_{chains} increases by 1.

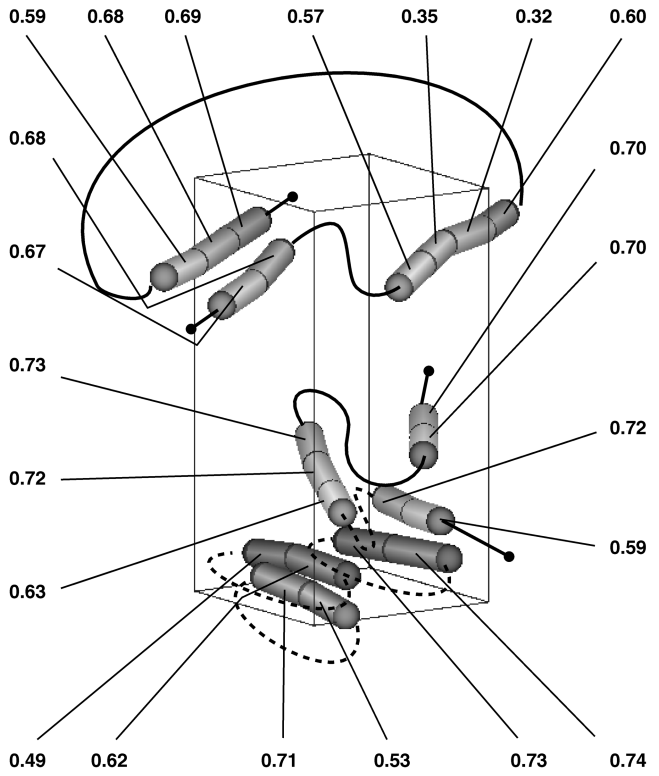

FIG. 9. The final chain conformation Ω, obtained by running the simulated annealing program on the last five configurations of the $T^*=0.8$ run, in the $N=21\,000$ system. For each segment, we show the goal function G_Γ. For clarity, twisted periodic boundary conditions have been applied to some segments to return them to the basic simulation cell: solid lines indicate segments which are actually joined, dotted lines show segments which are almost joined. Apparently free ends of chains are shown with lines terminating in a point.

The simulated annealing results for the final configurations at $T^*=0.8$ from the $N=21\,000$ simulations are shown in Fig. 9. There is qualitative agreement with the TGB defect structure in several key respects. In the majority of cases, the distribution of molecules around each segment corresponds with the twist defect structure. All of the segments found lie approximately in the xy plane, and their orientations follow the position of the peaks in the structure profile. The three defects at the bottom of the picture are oriented along the y axis. A grain boundary consisting of defects with separation $\ell_d=L_\perp/3$ and $d_0=4.3\sigma_0$ would give $\Delta\theta\approx 19°$, whereas the structure and director profiles show that the actual grain boundary angle is nearer 28°. This discrepancy is presumably due to other less well-defined defects, or nematic regions, involved in this boundary that are not detected by our program. Finally, considering only segments around which the ordering is convincingly helical, the total length of defect segments found in this particular configuration is $295\sigma_0$, compared to $\pi L_\perp^2/2d_0=570\sigma_0$, i.e., slightly more than half of the total amount of twist in the simulation cell is explained by the presence of well-defined twist defects found by our annealing program.

TABLE II. Parameters used in the simulated annealing program.

Number of attempted moves n_{steps}	10^6
Number of segments	22
Maximum total defect length $L_{\max}$	$600\sigma_0$
Bounds on segment length: $\ell_{\min}<\ell_\Gamma<\ell_{\max}$	$10\sigma_0<\ell_\Gamma<L_\perp/2$
Chain weight λ	40
Initial annealing temperature τ_0	40
Cutoff radii for $\mathcal{R}_\Gamma$: $r_{\min}<r<r_{\max}$	$2\sigma_0<r<5.5\sigma_0$

We also analyzed the final configurations from the $N=84\,000$ runs at $T^*=0.9$, and here too we found many segments which correspond to well-defined defects. The distribution of these segments is shown in Fig. 10, and the molecular arrangement in the neighborhood of a typical example in Fig. 11. The results are qualitatively similar to those described above. Interestingly, in this case the distribution of defects along the z axis is more uniform. This is consistent with the structure profiles in Fig. 5(c), where we see that there is a large degree of local smectic ordering, and yet it is difficult to identify grain boundaries at specific values of z. This does not simply indicate that the intrinsic grain-boundary width is larger for $N=84\,000$ than for $N=21\,000$: the apparent width will also be larger due to the greater scope for fluctuations away from the idealized case of a planar interface, perfectly normal to the twist axis.

VI. DISCUSSION AND CONCLUSIONS

We have performed extensive large-scale molecular-dynamics simulations of a system of particles interacting via a particular parametrization of the Gay-Berne potential. In order to represent the effects of molecular chirality (or an

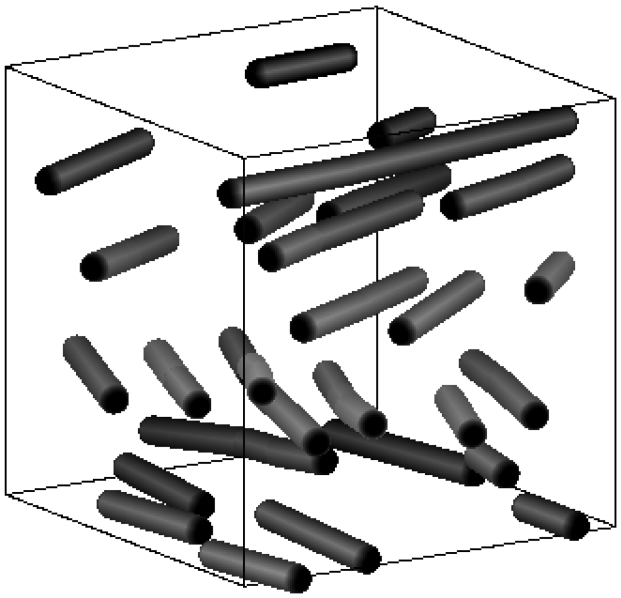

FIG. 10. The distribution of segments from the simulated annealing analysis of configurations from the end of the $T^*=0.9$, $N=84\,000$ run. Only segments which clearly correspond to defects are shown.

externally applied torque), twisted periodic boundary conditions were used. Starting from a twisted nematic phase, we investigated the structure that forms on lowering the temperature below that of the $N \rightarrow S_A$ transition in the untwisted system. We calculated profiles to characterize the variation of orientational and translational ordering along the twist axis. These results indicate the development of several smecticlike domains, which at lower temperatures are separated by well-defined grain boundaries. To this extent, the structure we observe corresponds with that of the twist grain-boundary (TGB) phase. In order to study the interfacial regions, we have developed a technique for locating line defects in molecular configurations, based on simulated annealing. By using this in conjunction with an appropriate goal function, we have attempted to characterize the distribution of twist defects. Again, bearing in mind the limited system size and the very long time scale for motion of defects, the nature and distribution of defects observed in our simulation is in good qualitative agreement with the TGB structure. The pitch of the twist we apply to our system, and other key physical parameters, are in reasonable agreement with experimental results [6], and are summarized in Table III.

We have observed the TGB phase to form *spontaneously* on cooling a uniformly twisted nematic phase, but the time scales involved are quite long: it is reasonable to ask whether the observed structure might reflect the initial conditions, or perhaps that, having formed, it might relax to a different structure, given sufficient time. To give more confidence in the results, we have conducted additional simulations. First, we have conducted a quench for the $N=21\,000$ system from $T^*=1.0$ to $T^*=0.9$, starting from a twisted nematic phase prepared completely independently from the original simulations. After 88 000 MD time steps, the initial stages of TGB structure formation are clearly evident. Second, to investigate the possibility that our MD method might artificially

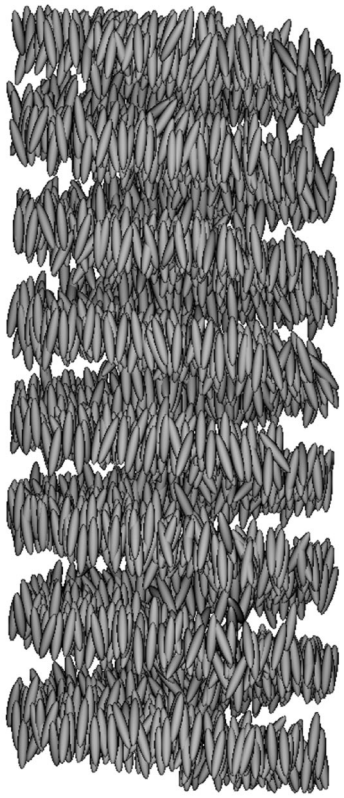

FIG. 11. The arrangement of molecules within a cylinder of radius $7\sigma_0$ coaxial with a typical segment, in the $N=84\,000$ system. The molecules are reduced in size for clarity.

stabilize the TGB phase in some way, we have conducted Monte Carlo simulations of the $N=21\,000$ system, at $T^*=0.9$, starting from the final configurations of the original MD runs at this temperature. After 20 000 MC attempted moves per particle, no change at all in the TGB domain structure is seen. Ideally, we would like to repeat and extend these simulations, but we are limited by the expense of simulating such large systems.

If the simulation time scale could be extended significantly (and this would almost certainly mean abandoning the molecular-dynamics description in favor of a more coarse-grained scheme) our simulated annealing technique could also be used to investigate the *dynamics* of defects. Their motion could be tracked from one density distribution to the next by means of short annealing runs at low annealing temperature. We did not do this because our runs are much too short (of the order of nanoseconds in real time); our director and structure profiles at $T^*=0.9$ and 0.8 do not change ap-

TABLE III. Comparison of key physical parameters of system with the experimental results of Goodby *et al.* [2].

Property	Simulation (units of σ_0)	Experiment (nm)
Smectic layer spacing d_0	4.3	4.1
Helix pitch λ	320	500
Smectic domain size ℓ_s	20	24
Dislocation line separation ℓ_d	11	15

preciably once the domains have formed, and this suggests that the network of defects is fairly static on the time scale of the simulations which we have undertaken.

We should point out the limitations of the current work. We have not estimated the shift in the $N \rightarrow S_A$ transition temperature due to the imposed twist, which would be interesting to measure, but will require much longer runs. The degree of disorder in our systems should not be overlooked: despite our reference to the Renn-Lubensky theory, only about half of the twist in our systems is directly attributed to explicitly identified defects. Also, it is a fact that our system is only large enough to include a few grain boundaries, each of which contains a small number of screw dislocations. Further information could be obtained by brute-force simulations of larger systems for longer times, or by some combination of molecular modeling and continuum modeling.

ACKNOWLEDGMENTS

This research was supported by EPSRC to M.A.W., through the provision of computer hardware, and through an allocation of time on the Cray T3D at Edinburgh University under the High Performance Computing Initiative. We gratefully acknowledge the contributions of Bill Smith and Alain Sauron to the development of the GBMEGA code, and the assistance of Muataz Al-Barwani in conducting some of the runs.

[1] S. R. Renn and T. C. Lubensky, Phys. Rev. A **38**, 2132 (1988).
[2] J. W. Goodby *et al.*, Nature (London) **337**, 449 (1989).
[3] L. Navailles, P. Barois, and H. T. Nguyen, Phys. Rev. Lett. **71**, 545 (1993).
[4] Y. Galerne, Phys. Rev. Lett. **72**, 1299 (1994).
[5] L. Navailles, P. Barois, and H. T. Nguyen, Phys. Rev. Lett. **72**, 1300 (1994).
[6] K. J. Ihn *et al.*, Science **258**, 275 (1992).
[7] J. S. Patel, Phys. Rev. E **49**, R3594 (1994).
[8] S. Fraden, in *Observation, Prediction and Simulation of Phase Transitions in Complex Fluids*, Vol. 460 of *NATO ASI Series C*, edited by M. Baus, L. F. Rull, and J.-P. Ryckaert (Kluwer, Dordrecht, 1995), pp. 113–164, proceedings of the NATO Advanced Study Institute on ''Observation, prediction and simulation of phase transitions in complex fluids,'' Varenna, Italy, July 25–August 5, 1994.
[9] M. R. Wilson *et al.*, J. Comput. Chem. **18**, 478 (1997).
[10] J. G. Gay and B. J. Berne, J. Chem. Phys. **74**, 3316 (1981).
[11] G. R. Luckhurst, R. A. Stephens, and R. W. Phippen, Liq. Cryst. **8**, 451 (1990).
[12] E. de Miguel *et al.*, Mol. Phys. **72**, 593 (1991).
[13] R. Berardi, A. P. J. Emerson, and C. Zannoni, J. Chem. Soc., Faraday Trans. **89**, 4069 (1993).
[14] M. Bates, private communication.
[15] M. P. Allen and D. J. Tildesley, *Computer Simulation of Liquids* (Clarendon, Oxford, 1987).
[16] M. P. Allen and A. J. Masters, Mol. Phys. **79**, 277 (1993).
[17] W. H. Press, B. P. Flannery, S. A. Teukolsky, and W. T. Vetterling, *Numerical Recipes* (Cambridge University Press, Cambridge, 1986).